Fiber networks amplify active stress

Pierre Ronceray[a], Chase P. Broedersz[b,c,1], and Martin Lenz[a,1]

[a]Laboratoire de Physique Théorique et Modèles Statistiques (LPTMS), CNRS, Université Paris-Sud, Université Paris-Saclay, 91405 Orsay, France; [b]Arnold-Sommerfeld-Center for Theoretical Physics and Center for NanoScience, Ludwig-Maximilians-Universität München, D-80333 Munich, Germany; and [c]Lewis-Sigler Institute for Integrative Genomics and Joseph Henry Laboratories of Physics, Princeton University, Princeton, NJ 08544

Edited by Tom C. Lubensky, University of Pennsylvania, Philadelphia, PA, and approved December 18, 2015 (received for review July 20, 2015)

Large-scale force generation is essential for biological functions such as cell motility, embryonic development, and muscle contraction. In these processes, forces generated at the molecular level by motor proteins are transmitted by disordered fiber networks, resulting in large-scale active stresses. Although these fiber networks are well characterized macroscopically, this stress generation by microscopic active units is not well understood. Here we theoretically study force transmission in these networks. We find that collective fiber buckling in the vicinity of a local active unit results in a rectification of stress towards strongly amplified isotropic contraction. This stress amplification is reinforced by the networks' disordered nature, but saturates for high densities of active units. Our predictions are quantitatively consistent with experiments on reconstituted tissues and actomyosin networks and shed light on the role of the network microstructure in shaping active stresses in cells and tissue.

soft active matter | fiber networks | cytoskeleton | biological tissues

Living systems constantly convert biochemical energy into forces and motion. In cells, forces are largely generated internally by molecular motors acting on the cytoskeleton, a scaffold of protein fibers (Fig. 1*A*). Forces from multiple motors are propagated along this fiber network, driving numerous processes such as mitosis and cell motility (1) and allowing the cell as a whole to exert stresses on its surroundings. At the larger scale of connective tissue, many such stress-exerting cells act on another type of fiber network known as the extracellular matrix (Fig. 1*B*). This network propagates cellular forces to the scale of the whole tissue, powering processes such as wound healing and morphogenesis. Despite important differences in molecular details and length scales, a common physical principle thus governs stress generation in biological matter: Internal forces from multiple localized "active units"—motors or cells—are propagated by a fiber network to generate large-scale stresses. However, a theoretical framework relating microscopic internal active forces to macroscopic stresses in these networks is lacking. Here we propose such a theory for elastic networks.

This generic stress generation problem is confounded by the interplay of network disorder and nonlinear elasticity. Active units generate forces at the scale of the network mesh size, and force transmission to larger scales thus sensitively depends on local network heterogeneities. In the special case of linear elastic networks, the macroscopic active stress is simply given by the density of active force dipoles, irrespective of network characteristics (2). Importantly, however, this relationship is not applicable to most biological systems, because typical active forces are amply sufficient to probe the nonlinear properties of their constitutive fibers, which stiffen under tension and buckle under compression (3). Indeed, recent experiments on reconstituted biopolymer gels have shown that individual active units induce widespread buckling and stiffening (4, 5), and theory suggests that such fiber nonlinearities can enhance the range of force propagation (6, 7).

Fiber networks also exhibit complex, nonlinear mechanical properties arising at larger scales, owing to collective deformations favored by the networks' weak connectivity (3, 8). The role of connectivity in elasticity was famously investigated by Maxwell, who noticed that a spring network in dimension d becomes mechanically unstable for connectivities $z < 2d$. Interestingly, most biological fiber networks exhibit connectivities well below this threshold and therefore cannot be stabilized solely by the longitudinal stretching rigidity of their fibers. Instead, their macroscopic mechanical properties are typically controlled by the fiber bending rigidity (9). In contrast to stretching-dominated networks with connectivities above the Maxwell threshold, such weakly connected, bending-dominated networks are soft and extremely sensitive to mechanical perturbations (9–11). In these networks, stresses generated by active units propagate along intricate force chains (12, 13) whose effects on force transmission remain unexplored. Collections of such active units generate large stresses, with dramatic effects such as macroscopic network stiffening (14–16) and network remodeling (5, 17).

Here we study the theoretical principles underlying stress generation by localized active units embedded in disordered fiber networks (Fig. 1*C*). We find that arbitrary local force distributions generically induce large isotropic, contractile stress fields at the network level, provided that the active forces are large enough to induce buckling in the network. In this case, the stress generated in a biopolymer network dramatically exceeds the stress level that would be produced in a linear elastic medium (2), implying a striking network-induced amplification of active stress. Our findings elucidate the origins and magnitude of stress amplification observed in experiments on reconstituted tissues (4, 18) and actomyosin networks (14, 17). We thus provide a conceptual framework for stress generation in biological fiber networks.

A Lattice Model for Elastic Fiber Networks

We investigate force transmission, using a lattice-based fiber network model (3). In our model, straight fibers are connected at each lattice vertex by cross-links that do not constrain their relative angles. Each lattice edge represents a "bond" made of two straight segments and can thus stretch, bend, or buckle (Fig. 1*D* and Fig. S1). Segments have stretching rigidity μ and a rest length equal to one, implying a stretching energy $\mu(\ell-1)^2/2$ per segment of length ℓ. The fiber bending rigidity is set to unity by penalizing angular deflections θ between consecutive segments

Significance

Living organisms generate forces to move, change shape, and maintain their internal functions. These forces are typically produced by molecular motors embedded in networks of fibers. Although these motors are traditionally regarded as the defining elements of biological force generation, here we show that the surrounding network also plays a central role in this process. Indeed, rather than merely propagating forces like a simple elastic medium, fiber networks produce emergent, dramatically amplified stresses and can go so far as reversing small-scale extensile forces into large-scale contraction. Our theory quantitatively accounts for experimental measurements of contraction.

Author contributions: P.R., C.P.B., and M.L. designed research, performed research, analyzed data, and wrote the paper.

The authors declare no conflict of interest.

This article is a PNAS Direct Submission.

[1]To whom correspondence may be addressed. Email: martin.lenz@u-psud.fr or c.broedersz@lmu.de.

This article contains supporting information online at www.pnas.org/lookup/suppl/doi:10.1073/pnas.1514208113/-/DCSupplemental.

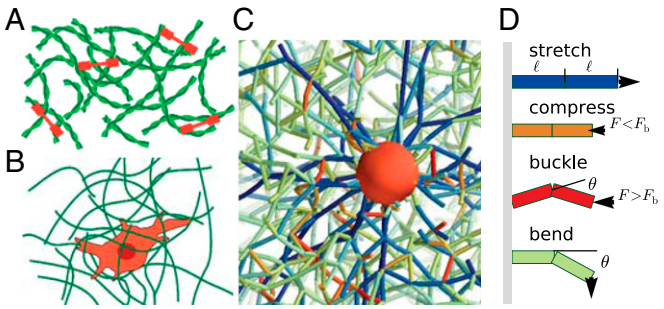

Fig. 1. Biological fiber networks (green) transmit forces generated by localized active units (red). (*A*) Myosin molecular motors exert forces on the actin cytoskeleton. (*B*) Contractile cells exert forces on the extracellular matrix. (*C*) The large nonlinear deformations induced by a model active unit in the surrounding fiber network result in stress amplification, as shown in this paper. Fiber color code is shown in *D*. (*D*) Each bond in the network comprises two rigid segments hinged together to allow buckling.

through a bending energy $2\sin^2(\theta/2)$. Consequently, individual bonds buckle under a critical force $F_b = 1$, and we consider nearly inextensible fibers by assuming $\mu \gg 1$ (henceforth we use $\mu = 10^3$).

Network disorder is introduced through bond depletion, i.e., by randomly decimating the lattice so that two neighboring vertices are connected by a bond with probability p. This probability controls the network's connectivity, giving rise to distinct elastic regimes delimited by two thresholds p_{cf} and p_b. The network is stretching dominated for $p > p_{cf}$, bending dominated for $p_b < p < p_{cf}$, and mechanically unstable for $p < p_b$. Here we consider 2D hexagonal lattices, for which $p_b \simeq 0.45$ and $p_{cf} \simeq 0.65$, and 3D face-centered cubic lattices with $p_b \simeq 0.27$ and $p_{cf} \simeq 0.47$. Because the network displays singular behavior in the vicinity of p_b and p_{cf}, here we focus our investigations on the generic stretching- and bending-dominated regimes away from these critical points (9).

We model active units as local sets of forces $\mathbf{F}_i$ exerted on network vertices i with positions $\mathbf{R}_i$. We impose that the total force and torque exerted by such units vanish, as expected if the active units are not subjected to any external force. We consider networks at mechanical equilibrium under the influence of these forces. We denote by σ the trace (i.e., the isotropic component) of the coarse-grained active stress induced in the fiber network by a density ρ of such units.

The relationship between this active stress and local forces in homogeneous linear networks is very simple and yields (2)

$$\sigma = \sigma_{\text{lin}} = -\rho \mathcal{D}_{\text{loc}}, \qquad [1]$$

where $\mathcal{D}_{\text{loc}} = \sum_i \mathbf{F}_i \cdot \mathbf{R}_i$ is the dipole moment of the forces associated with a single active unit. Eq. **1** is generically violated in disordered or nonlinear networks, although it holds on average in linear networks with homogeneous disorder

$$\langle \sigma \rangle = \sigma_{\text{lin}}, \qquad [2]$$

where $\langle \cdot \rangle$ denotes the average over disorder (2). To quantify violations of Eq. **1**, we define the far-field force dipole $\mathcal{D}_{\text{far}}$ through the relation

$$\sigma = -\rho \mathcal{D}_{\text{far}} \quad \Rightarrow \quad \frac{\mathcal{D}_{\text{far}}}{\mathcal{D}_{\text{loc}}} = \frac{\sigma}{\sigma_{\text{lin}}}. \qquad [3]$$

Conceptually, this far-field dipole characterizes the apparent strength of an individual active unit renormalized by force transmission in the disordered, nonlinear network. It quantifies how contractile ($\mathcal{D}_{\text{far}} < 0$) or extensile ($\mathcal{D}_{\text{far}} > 0$) the active medium is, and the dipole amplification ratio $\mathcal{D}_{\text{far}}/\mathcal{D}_{\text{loc}}$ (or equivalently the stress amplification ratio $\sigma/\sigma_{\text{lin}}$) measures the deviation from linear homogeneous force transmission.

Contractility Robustly Emerges from Large Local Forces

Stress generation by active units integrates mechanical contributions from a range of length scales. We first consider the immediate vicinity of the active unit. Network disorder plays a crucial role at that scale, because forces are transmitted through a random pattern of force lines determined by the specific configuration of depleted bonds (Fig. 2 *A* and *B*, *Insets*). To understand how these patterns affect force transmission, we investigate the probability distribution of the far-field force dipole $\mathcal{D}_{\text{far}}$ for simple active units consisting of two equal and opposite point forces of magnitude F_0.

We first consider the linear regime $F_0 \ll F_b$, where the average dipole amplification equals unity: $\langle \mathcal{D}_{\text{far}}/\mathcal{D}_{\text{loc}} \rangle = 1$ (Eqs. **2** and **3**). The fluctuations around this average are strikingly broad compared with this average, shown by plotting the distribution of dipole amplifications (Fig. 2 *A* and *B*). For instance, a significant fraction (37%) of all network geometries yield negative amplification, i.e., an effective extensility in response to a contractile dipole (Fig. 2*A*, *Inset*). Due to linearity, contractility in response to an extensile dipole is just as likely. Overall, the far-field response in the linear regime is only loosely correlated to the applied force dipole.

The situation is dramatically different in the large force regime ($F_0 \gg F_b$), where fibers buckle and induce nonlinear network response. This is illustrated by the distributions of dipole amplifications in two opposite cases: a large contractile and a large extensile force dipole (Fig. 2 *C* and *D*). Although the detailed shapes of these curves are model dependent, three robust features emerge: First, locally extensile dipoles predominantly undergo negative amplification, implying far-field contractility irrespective of the sign of $\mathcal{D}_{\text{loc}}$ (as in, e.g., Fig. 2*D*, *Inset*). Second, the randomization observed in the linear regime is strongly attenuated, and the sign of the amplification is very reproducible (positive for 98% of the contractile dipoles and negative for 86% of the extensile ones). Third, the magnitude of the average amplification is significantly larger than one (in Fig. 2 *C* and *D*, $\langle \mathcal{D}_{\text{far}}/\mathcal{D}_{\text{loc}} \rangle = 6.9$ and -3.2 for contractile and extensile dipoles, respectively).

To understand these three effects, we consider contractile and extensile dipoles in a simpler regular network (no bond depletion, Fig. 2 *E* and *F*). Qualitatively, these uniform networks behave similarly to the randomly depleted ones described above: Force dipole conservation holds for $F_0 \ll F_b$, whereas for $F_0 \gg F_b$ dipoles are rectified toward contraction and their magnitude is amplified (Fig. 2*G*). The origin of these behaviors is apparent from the spatial arrangement of the forces in Fig. 2 *E* and *F*. Whereas contractile and extensile active units both induce compressive and tensile stresses in their immediate surroundings, the buckling of the individual bonds prevents the long-range propagation of the former. This results in enhanced tensile stresses in the far field and thus in strongly contractile far-field dipoles. In addition, this nonlinear response renders the far-field stresses uniformly tensile and therefore more isotropic than the active unit forces. We quantify this effect in Fig. 2*G*, *Inset*, using an anisotropy parameter for the far-field stresses $1 - (\sum_\mu \sigma^{\mu\mu})^2/(d \sum_{\mu,\nu} \sigma^{\mu\nu}\sigma^{\nu\mu})$, where d is the dimension of space and $\sigma^{\mu\nu}$ is the coarse-grained active stress tensor of the active medium (*Supporting Information*). This anisotropy parameter indeed becomes very small for large local dipoles of either sign as shown in Fig. 2*G*.

Moving to a systematic quantification of force transmission in depleted, bending-dominated networks, we show in Fig. 2 *H* and *I* the same three effects of rectification, amplification, and isotropization, which set in at smaller forces than in regular networks. Overall, these effects are very general and hold in both bending- and stretching-dominated depleted networks, in two and three dimensions, and for active units with complicated force distributions not along lattice directions (Figs. S3 and S4). Thus, beyond the immediate neighborhood of the active force-generating unit, strong isotropic

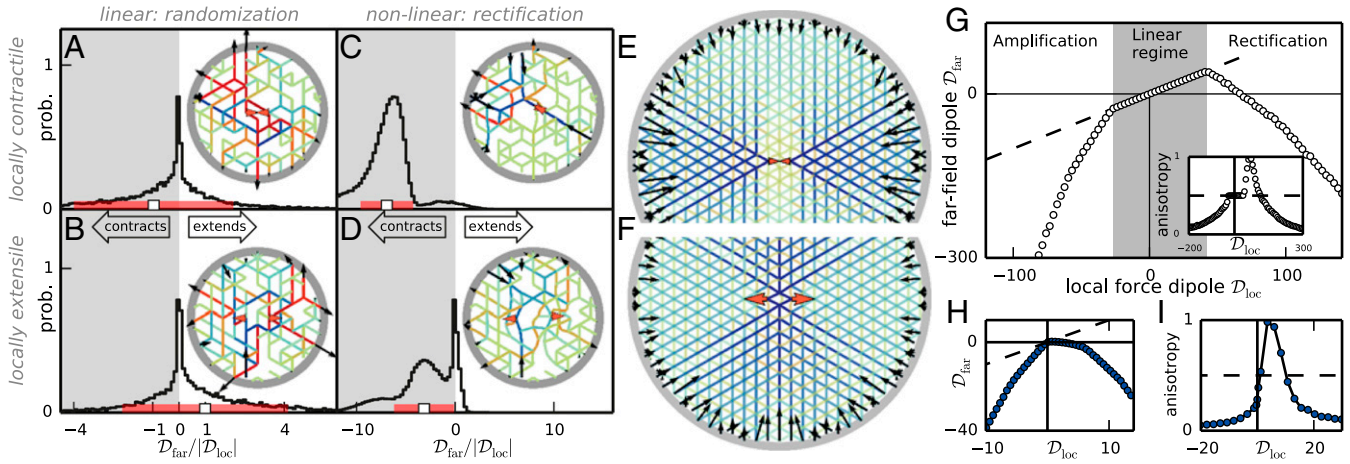

Fig. 2. Network buckling converts active forces into emergent isotropic contraction over a few mesh sizes. (*A* and *B*) In the linear response regime ($F_0 \ll F_b$), the far-field dipole $\mathcal{D}_{far}$ exhibits a broad distribution with average $\mathcal{D}_{loc}$ (histogram; the gray and white areas correspond to contractile and extensile systems, respectively). The square and the red bars indicate the mean and standard deviation of the distribution. *Insets* show contractile and extensile active forces (red arrowheads) propagate along a complex network of force lines (blue, tension; red, compression), resulting in randomized force distributions at a fixed boundary (black arrows). (*C* and *D*) At larger forces (here $F_0 = 20F_b$), both contractile and extensile dipoles typically result in contractile forces at the boundary ($\mathcal{D}_{far} < 0$). The corresponding distributions of amplifications are narrower than in the linear case. (*E* and *F*) Regular networks subjected to large ($F_0 = 500F_b$) local dipoles of either sign exert uniformly contractile forces on the fixed boundary. (*G*) Corresponding far-field dipole as a function of the local dipole, showing amplification and rectification in the nonlinear regime. The dashed line indicates the linear prediction $\mathcal{D}_{far} = \mathcal{D}_{loc}$. *Inset* shows stress anisotropy parameter (defined in the main text) as a function of the local dipole. (*H* and *I*) Far-field dipole and anisotropy as a function of the local dipole in a bending-dominated 2D network. Parameters: $\mu = 10^3$; for depleted networks $p = 0.6$, averages over 10^4 samples.

contractile stresses emerge in the system from a generic local force distribution due to the nonlinear force propagation properties of the fiber network.

A Model for Active Units as Isotropic Pullers

Whereas nonlinear force transmission over large length scales involves large active forces, the model for active units used above can exert only moderate dipoles in soft, weakly connected networks. Indeed, for large enough contractile dipoles the two vertices on which the forces are applied collapse to a point as in Fig. 2*C*, *Inset*, preventing further contraction. In contrast, molecular motors and contractile cells continuously pull fibers in without collapsing. To study the response of fiber networks to large active forces, we thus introduce an active unit model capable of exerting arbitrarily large forces without changing its size. We assume an isotropic force distribution, an approximation valid in the large force regime, where complicated force distributions are locally rectified toward isotropic contraction by the network (Fig. 2 *G* and *I*).

Our model active unit is centered on a vertex i and pulls on every vertex j within a distance $2R_0$ with a radial force

$$\mathbf{F}_{ij} = \begin{cases} -F_0 \dfrac{r_{ij}}{R_0}\hat{\mathbf{r}}_{ij} & \text{if } r_{ij} < R_0 \\ -F_0\left(2 - \dfrac{r_{ij}}{R_0}\right)\hat{\mathbf{r}}_{ij} & \text{if } R_0 \le r_{ij} < 2R_0 \end{cases}, \qquad [4]$$

where F_0 is the maximum force exerted by the unit on a vertex, r_{ij} is the distance between i and j, and $\hat{\boldsymbol{r}}_{\boldsymbol{ij}}$ is the associated unit vector. A strong active unit in a soft network may pull in many fibers, exerting a force $\approx F_0$ on each of them. Adding the contributions of all these fibers results in a large local dipole, the magnitude of which is not well reflected by the value of F_0. The influence of the active unit on the surrounding network is better characterized by the force F, which we define as the average force per unit area exerted on the surrounding network by the active unit at its outer surface ($r = 2R_0$). These isotropically pulling units are thus suited to the study of arbitrarily large active forces, and we use them in the remainder of this article.

Contractile Forces Are Long Ranged in Bucklable Media

We now study force propagation beyond the immediate vicinity of an active unit, using the above-described isotropic puller. We identify two asymptotic regimes for this propagation. Close to the active unit, forces are large and fiber buckling affects force transmission, whereas beyond a crossover distance R^* forces are weak and linear elasticity prevails.

To describe the near-field regime, we note that fiber buckling prevents the network from sustaining compressive stresses above the buckling threshold. Close to the active unit, the network is thus effectively equivalent to a network of floppy ropes, i.e., filaments with tensile strength but no resistance to compression or bending. The active unit pulls on these ropes and thus becomes the center of a radial arrangement of tensed ropes. Force balance on a small portion of a spherical shell centered on the active unit imposes that radial stresses in this rope-like medium decay as

$$\sigma_{rr}(r) \propto r^{-(d-1)}, \quad r \ll R^*, \qquad [5]$$

where r is the distance from the active unit and d the dimension of space (19). In the far field, stresses are small and buckling does not occur, implying that force transmission crosses over from rope-like to linear elasticity:

$$\sigma_{rr}(r) \propto r^{-d}, \quad r \gg R^*. \qquad [6]$$

Stress decay is thus significantly slower in the rope-like near field than in the linear far field, leading to an increased range for force transmission (7). Conceptually, the faster decay in a linear elastic medium can again be understood by balancing forces on a fraction of spherical shell centered on the active unit, where radial stresses are now partially compensated by orthoradial stresses. We expect that the crossover between these two regimes occurs when radial stresses are comparable to the buckling stress, implying that the crossover length depends on the active force:

$$R^* \approx R_0 \left(\frac{F}{F_b}\right)^{1/(d-1)}. \quad [7]$$

To test this two-regime scenario, we simulate force propagation away from a single active unit in both stretching- and bending-dominated networks in two and three dimensions. In all cases, rope-like radial stresses and bond buckling are predominant in the vicinity of the active unit (Fig. 3 *A*–*C*). Monitoring the decay of radial stresses with r, we find a crossover from rope-like to linear behavior, consistent with Eqs. **5** and **6** (Fig. 3 *D*, *F*, and *H*).

Visually, the crossover length R^* coincides with the outer boundary of the radially tensed, buckling-rich region (Fig. 3 *A*–*C*, black circles). In stretching-dominated networks, our prediction of Eq. **7** captures the force dependence of this crossover length (Fig. 3*E* and Fig. S5). In contrast, bending-dominated networks display a more complex behavior: Although the system still exhibits a transition from rope-like to linear force transmission, the crossover region is much broader (Fig. 3 *F* and *H*) and rope-like force transmission extends much farther than predicted by Eq. **7**. Instead, we find behavior that is reasonably well described by a power law $R^* \propto F^\alpha$ with anomalous exponents $\alpha \approx 0.4$ in 2D and $\alpha \approx 0.25$ in 3D (Fig. 3 *G* and *I*). These exponents appear to be insensitive to the exact value of the depletion parameter p within the bending-dominated regime (Fig. S5). We speculate that this extended range for nonlinear force transmission is mediated by the strong concentration of tensile stresses along force chains (12, 20) observed in Fig. 3 *B* and *C*. Indeed, such force chains are much more pronounced in bending-dominated than in stretching-dominated networks (Fig. S5). The difference between stretching- and bending-dominated exponents thus suggests that these elastic heterogeneities qualitatively affect force transmission in such soft networks. As a result, contractile forces large enough to induce buckling benefit from an enhanced range of transmission, characterized by the mesoscopic radius of the rope-like region R^*.

Amplification by a Collection of Active Units

Over large length scales, active stresses in biological systems are generated by multiple active units. We thus compute the stress amplification ratio in the presence of a finite density of randomly positioned active units in 2D and 3D for various densities ρ and depletion parameters p (Fig. 4*A*). In all cases we observe three stress amplification regimes as a function of the unit force F: a low-force plateau without amplification, an intermediate regime of increasing amplification, and a saturation of the amplification at a level that depends on ρ.

In the low-force regime, linear force transmission prevails (Fig. 4*B*) and the active stress is given by Eq. **1**:

$$\sigma = \sigma_{\text{lin}} = -\rho \mathcal{D}_{\text{loc}} \approx \rho F R_0. \quad [8]$$

For moderate forces, the fibers in the network buckle in the vicinity of each active unit, up to a distance R^*. Individual units are thus typically surrounded by nonoverlapping nonlinear regions of size R^*, as illustrated in Fig. 4*C*. To predict the resulting active stress in the system, we model each nonlinear region as an effective active unit of size R^* and force dipole $\mathcal{D}_{\text{eff}} \approx -FR^*$, where we use Eq. **5** to describe force propagation within the nonlinear region. As the effective units are themselves embedded in a linear medium, linear force transmission (Eq. **1**) outside of these units implies

$$\sigma \approx -\rho \mathcal{D}_{\text{eff}} \approx \rho F R^*. \quad [9]$$

We thus predict that stress amplification in this regime scales as $\sigma/\sigma_{\text{lin}} \approx R^*/R_0$. We confirm this prediction in Fig. 4*E*. Because R^* increases with the active unit force in this regime, the large-scale stress amplification $\sigma/\sigma_{\text{lin}}$ increases with F as previously observed in Fig. 4*A*.

For large forces, the radius of the rope-like regions becomes so large as to exceed the typical distance between adjacent

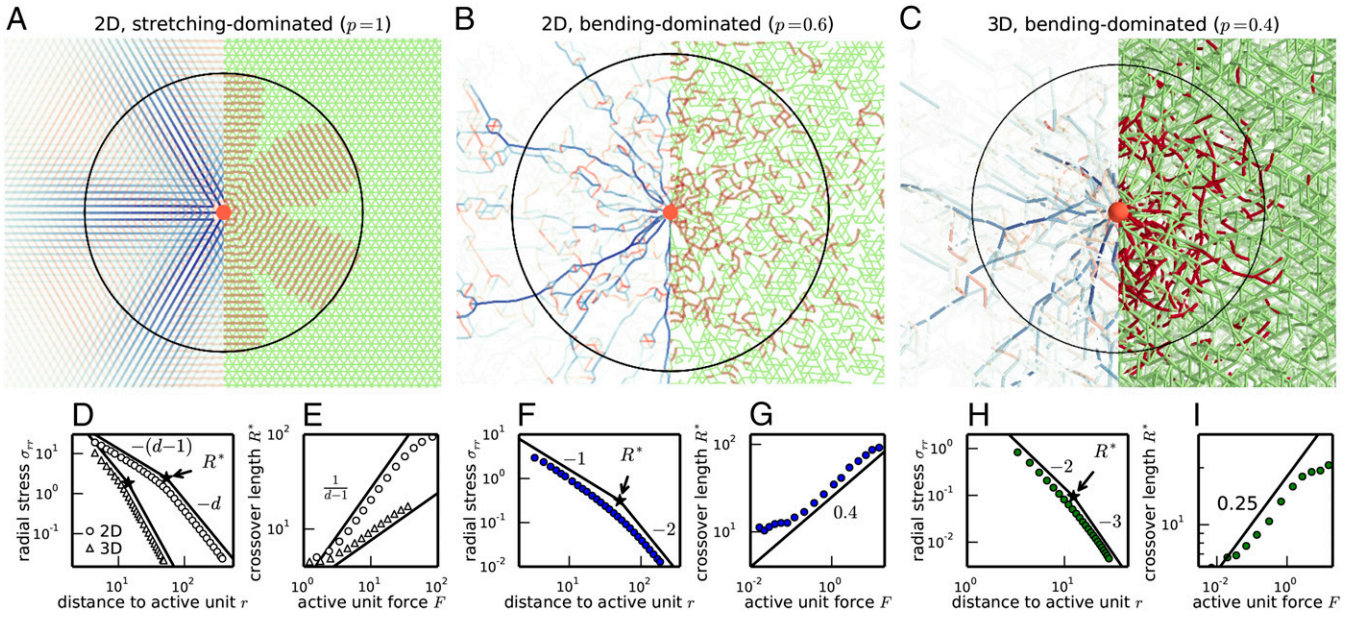

Fig. 3. Nonlinear network behavior enhances the range over which stresses are transmitted. (*A*–*C*) A localized, isotropically pulling active unit (red circle of radius $R_0 = 1.95$) induces stress lines (*A*–*C*, *Left*: blue, tension; red, compression) and buckling (*A*–*C*, *Right*: red, buckling; green, nonbuckled bonds) in the surrounding fiber network. Black circle: radius R^* of the rope-like region. *C* shows a slice of a 3D system. (*D*, *F*, and *H*) Decay of the average radial stress in the network (corrected for boundary effects) (*Supporting Information* and Fig. S2) as a function of the distance to the active unit. Fitting the curve with the power laws of Eqs. **5** and **6** yields a measure of the crossover radius R^*. (*E*, *G*, and *I*) We tentatively describe the dependence of the crossover radius on active unit force by a power law (solid line) in the intermediate-F regime where it is not complicated by finite size effects due to either the active unit size (at small F) or that of the system boundary (at large F). Results were obtained in a 2D circular (3D spherical) network of radius 200 with fixed boundaries and averaged over 100 samples for disordered networks.

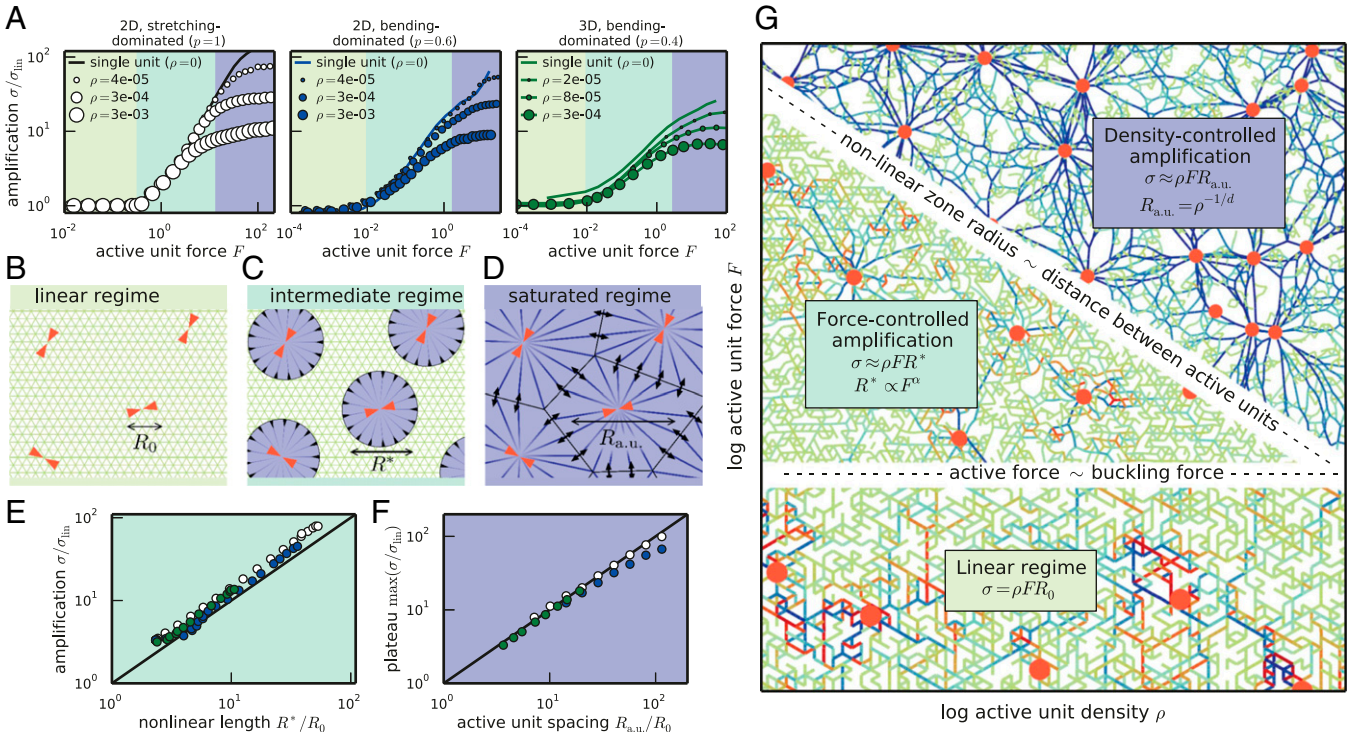

Fig. 4. Force transmission in the presence of a finite density ρ of active units. (*A*) Fiber networks in different dimensions and elastic regimes all display three stress amplification regimes as a function of active unit density and force, as suggested by the colored background. (*B–D*) Schematics of the network structure in each regime. The low-force linear regime (*B*) transitions to a regime of nonoverlapping nonlinear regions (*C*) as soon as *F* is sufficient to induce buckling. These nonlinear regions grow with increasing *F*, and amplification saturates as they start overlapping, which turns the whole network into a rope network (*D*). (*E*) In the intermediate-force regime, the stress amplification ratio is equal to the ratio R^*/R_0 as predicted by Eq. **9**. Color code as in *A*. (*F*) In the large-force regime, the stress amplification ratio is equal to the ratio $R_{\rm a.u.}/R_0$ as predicted by Eq. **10**. (*G*) Schematic phase diagram indicating the domain of applicability of the three stress amplification regimes, with representative snapshots of the corresponding systems in the background. Note that the picture described here is also valid for dense collections of anisotropic active units (Fig. S6).

active units $R_{\rm a.u.}=\rho^{-1/d}$. This causes the nonlinear regions associated to neighboring active units to overlap and renders the whole network mechanically equivalent to a collection of tensed, inextensible ropes whose geometry does not change significantly upon further increase of the force. To estimate the resulting network stress, we approximate the system as a mosaic of effective active units of size $R_{\rm a.u.}$ each with a force dipole $\mathcal{D}_{\rm eff}\approx -FR_{\rm a.u.}$ (Fig. 4*D*). This yields

$$\sigma\approx-\rho\mathcal{D}_{\rm eff}\approx\rho F R_{\rm a.u.}=\rho^{1-1/d}F. \qquad [10]$$

The resulting prediction for the stress amplification, $\sigma/\sigma_{\rm lin}\approx R_{\rm a.u.}/R_0$, is confirmed in Fig. 4*F*. Strikingly, the stress generated in this large-force regime has a nonlinear dependence on ρ, again consistent with Fig. 4*A*. Indeed, the addition or removal of active units leads to large rearrangements of the rope network, resulting in significant local modifications of force transmission.

We summarize the physics of collective stress generation by many active units in a phase diagram (Fig. 4*G*). In each regime, the magnitude of an active unit's effective force dipole is directly proportional to one of the three length scales R_0, R^*, and $R_{\rm a.u.}$ (Eqs. **8**–**10**). Whereas we have shown that R^* depends on the dimensionality and connectivity of the network, the other two length scales are purely geometrical. An important consequence of these findings is that the active stress generated in the associated regimes is essentially independent of the detailed properties of the fiber network.

Discussion

In living organisms, microscopic units exert active forces that are transmitted by fibrous networks to generate large-scale stresses. The challenge in analyzing this force-transmission problem stems from the disordered architecture of such fibrous networks and the nonlinearities associated with the strong forces exerted by biological active units. Despite this complexity, we find surprisingly simple and robust behaviors: In response to any distribution of active forces, dramatically amplified contractile stresses emerge in the network on large scales. This remarkable property hinges only on the local asymmetry in elastic response between tensed and compressed fibers and is enhanced by network disorder. Our

Table 1. Experimental data support stress amplification in fiber networks

System (source)	R_0, μm	$R_{\rm a.u.}$, μm	$R^*=R_0(F/F_b)^{1/(d-1)}$, μm	$\sigma_{\rm lin}$	$\sigma_{\rm th}$	$\sigma_{\rm exp}$
I: 3D actomyosin (14)	1	1	0.8 (linear regime)	12 Pa	12 Pa	14 Pa
II: 2D actomyosin (17)	1	20	15 (force controlled)	0.014 pN/μm	≥0.2 pN/μm	≥1 pN/μm
III: 3D blood clot (4, 18)	2	15	350 (density controlled)	9 Pa	70 Pa	150 Pa

The rope-like radius R^*, linear-theory active stress $\sigma_{\rm lin}$, and predicted amplified stress $\sigma_{\rm th}$ are computed using Eqs. **8**–**10** from independent estimates of the single-unit force *F* (*Supporting Information*) for comparison with the experimentally measured active stress $\sigma_{\rm exp}$. We use the stretching-dominated scaling for R^* (Eq. **7**), and thus the predicted active stress in system II is a lower bound as indicated by the ≥ symbol in the $\sigma_{\rm th}$ column; the ≥ in the $\sigma_{\rm exp}$ column reflects experimental uncertainties.

simple, yet realistic description of individual fibers yields a universal scenario for force transmission: long-ranged, rope-like propagation near a strong active unit and linear transmission in the far field. This generic result should be contrasted with recent studies focused on fibers with special singular force-extension relation (7) and resulting in nonuniversal force transmission regimes.

Our generic phase diagram (Fig. 4*G*) recapitulates our quantitative understanding of stress generation by a collection of active units based on the interplay between three length scales: active unit size R_0, rope-like length R^*, and typical distance between units $R_{\mathrm{a.u.}}$. To validate these predictions, we compare them with existing measurements on a broad range of in vitro systems (Table 1). We first consider system I, a dense 3D actin network with mesh size $\simeq 200$ nm in the presence of myosin motors, which assemble into so-called myosin thick filaments. A thick filament—which we consider as an individual active unit—exerts a typical force $F = 6$ pN, smaller than the buckling threshold $F_b \approx 10$ pN associated with a single 200-nm bond. This implies an active stress identical to the linear prediction, confirmed by the experimental result (14). We next consider system II, a 2D actin network bound to the outer surface of a lipid vesicle. The active units are essentially the same as in system I, but are much more sparsely distributed ($R_{\mathrm{a.u.}} \simeq 20$ μm). The network in system II is also much looser (mesh size $\simeq 1$ μm) than in system I, resulting in a much smaller bond buckling force. The combination of a low buckling threshold and a large spacing between active units leads us to predict a significant stress amplification $R^*/R_0 \simeq 15$ associated to the force-controlled regime (Fig. 4 *C* and *G*), in reasonable agreement with experiments (17). Finally, we consider a clot comprised of fibrin filaments and contractile platelets as active units (system III). The large forces exerted by platelets allow for long-range nonlinear effects, placing this in vitro system deep in the density-controlled regime (Fig. 4 *D* and *G*). Consequently, we expect stress amplification to be controlled by the distance between active units, irrespective of the large value of the active force $F \approx 10^4\, F_b$. We thus predict an amplification factor $R_{\mathrm{a.u}}/R_0 \simeq 8$, in good agreement with experimental data (4, 18). These three examples demonstrate our theory's ability to quantitatively account for stress amplification, and recent progress in the micromechanical characterization of active fiber networks opens promising perspectives for further exploring active stress amplification (4, 5, 17).

Far from merely transmitting active forces, we show that fiber networks dramatically alter force propagation as contractility emerges from arbitrary spatial distributions of local active forces. This could imply that living organisms do not have to fine-tune the detailed geometry of their active units, because any local force distribution yields essentially the same effects on large length scales. This emergence of contractility sheds a new light on the longstanding debate in cytoskeletal mechanics regarding the emergence of macroscopic contraction in nonmuscle actomyosin despite the absence of an intrinsic contractility of individual myosin motors (20–23). Indeed, although these motors exert equal amounts of local pushing and pulling forces (24, 25), our result suggests that the surrounding network rectifies pushing contributions into uniform contraction. This rectification effect in two and three dimensions contrasts with the behavior of previously studied one-dimensional actomyosin systems, where extensile dipoles are attenuated but not reversed (26). It complements more local effects biasing the effects of a motor toward contractility (25), such as local buckling (24) and polarity-induced treadmilling (27). More broadly, we suggest that this strong propensity for the emergence of contraction in fibrous materials can explain the overwhelming dominance of contractile stresses in active biological materials up to the tissue level. Clearly, this does not mean that it is impossible to generate large-scale expansion in living organisms as required for limb abduction and extension or for lung inflation. Nevertheless, in each of these examples the expansion actually results from the clever harnessing of muscle contraction through lever structures involving the skeleton. Our findings connect widely used phenomenological "active gel" theories (28) to the underlying molecular scale forces, a crucial step in bringing theory and experiments together in the study of active biological matter, and call for further progress in characterizing force transmission in fiber networks. For instance, whereas our results concern the short-time elastic response of the network, it will be interesting to see how they are modified on longer timescales as cross-linker detachment and cytoskeletal remodeling induce flow in the fibrous matrix.

ACKNOWLEDGMENTS. We thank Cécile Sykes and Guy Atlan for fruitful discussions. This work was supported by Marie Curie Integration Grant PCIG12-GA-2012-334053, "Investissements d'Avenir" LabEx PALM (ANR-10- LABX-0039-PALM), Agence Nationale de la Recherche Grant ANR-15-CE13-0004-03, and European Research Council Starting Grant 677532 (to M.L.), as well as by the German Excellence Initiative via the program "NanoSystems Initiative Munich" (NIM) and the Deutsche Forschungsgemeinschaft (DFG) via project B12 within the SFB 1032. P.R. is supported by "Initiative Doctorale Interdisciplinaire 2013" from IDEX Paris-Saclay (ANR-11-IDEX-0003-02), and C.P.B. is supported by a Lewis-Sigler fellowship. M.L.'s group belongs to the CNRS consortium CellTiss.

1. Blanchoin L, Boujemaa-Paterski R, Sykes C, Plastino J (2014) Actin dynamics, architecture, and mechanics in cell motility. *Physiol Rev* 94(1):235–263.
2. Ronceray P, Lenz M (2015) Connecting local active forces to macroscopic stress in elastic media. *Soft Matter* 11(8):1597–1605.
3. Broedersz CP, MacKintosh FC (2014) Modeling semiflexible polymer networks. *Rev Mod Phys* 86(3):995.
4. Lam WA, et al. (2011) Mechanics and contraction dynamics of single platelets and implications for clot stiffening. *Nat Mater* 10(1):61–66.
5. Murrell MP, Gardel ML (2012) F-actin buckling coordinates contractility and severing in a biomimetic actomyosin cortex. *Proc Natl Acad Sci USA* 109(51):20820–20825.
6. Shokef Y, Safran SA (2012) Scaling laws for the response of nonlinear elastic media with implications for cell mechanics. *Phys Rev Lett* 108(17):178103.
7. Notbohm J, Lesman A, Rosakis P, Tirrell DA, Ravichandran G (2015) Microbuckling of fibrin provides a mechanism for cell mechanosensing. *J R Soc Interface* 12(108):20150320.
8. Onck PR, Koeman T, van Dillen T, van der Giessen E (2005) Alternative explanation of stiffening in cross-linked semiflexible networks. *Phys Rev Lett* 95(17):178102.
9. Broedersz CP, Mao X, Lubensky TC, MacKintosh FC (2011) Criticality and isostaticity in fibre networks. *Nat Phys* 7:983–998.
10. Ulrich S, Upadhyaya N, van Opheusden B, Vitelli V (2013) Shear shocks in fragile networks. *Proc Natl Acad Sci USA* 110(52):20929–20934.
11. Wyart M, Liang H, Kabla A, Mahadevan L (2008) Elasticity of floppy and stiff random networks. *Phys Rev Lett* 101(21):215501.
12. Heussinger C, Frey E (2007) Force distributions and force chains in random stiff fiber networks. *Eur Phys J E Soft Matter* 24(1):47–53.
13. Head DA, Levine AJ, MacKintosh FC (2005) Mechanical response of semiflexible networks to localized perturbations. *Phys Rev E Stat Nonlin Soft Matter Phys* 72(6 Pt 1):061914.
14. Koenderink GH, et al. (2009) An active biopolymer network controlled by molecular motors. *Proc Natl Acad Sci USA* 106(36):15192–15197.
15. Jansen KA, Bacabac RG, Piechocka IK, Koenderink GH (2013) Cells actively stiffen fibrin networks by generating contractile stress. *Biophys J* 105(10):2240–2251.
16. Broedersz CP, MacKintosh FC (2011) Molecular motors stiffen non-affine semiflexible polymer networks. *Soft Matter* 7:3186–3191.
17. Carvalho K, et al. (2013) Cell-sized liposomes reveal how actomyosin cortical tension drives shape change. *Proc Natl Acad Sci USA* 110(41):16456–16461.
18. Jen CJ, McIntire LV (1982) The structural properties and contractile force of a clot. *Cell Motil* 2(5):445–455.
19. Rosakis P, Notbohm J, Ravichandran G (2015) A model for compression-weakening materials and the elastic fields due to contractile cells. *Journal of the Mechanics and Physics of Solids* 85:16–32.
20. Dasanayake NL, Michalski PJ, Carlsson AE (2011) General mechanism of actomyosin contractility. *Phys Rev Lett* 107(11):118101.
21. Sekimoto K, Nakazawa H (1998) *Current Topics in Physics* (World Scientific, Singapore), Vol 1.
22. Mizuno D, Tardin C, Schmidt CF, Mackintosh FC (2007) Nonequilibrium mechanics of active cytoskeletal networks. *Science* 315(5810):370–373.
23. Murrell M, Oakes PW, Lenz M, Gardel ML (2015) Forcing cells into shape: The mechanics of actomyosin contractility. *Nat Rev Mol Cell Biol* 16(8):486–498.
24. Lenz M, Gardel ML, Dinner AR (2012) Requirements for contractility in disordered cytoskeletal bundles. *New J Phys* 14:033037.
25. Lenz M (2014) Geometrical origins of contractility in disordered actomyosin networks. *Phys Rev X* 4:041002.
26. Lenz M, Thoresen T, Gardel ML, Dinner AR (2012) Contractile units in disordered actomyosin bundles arise from F-actin buckling. *Phys Rev Lett* 108(23):238107.
27. Mendes Pinto I, Rubinstein B, Kucharavy A, Unruh JR, Li R (2012) Actin depolymerization drives actomyosin ring contraction during budding yeast cytokinesis. *Dev Cell* 22(6):1247–1260.
28. Prost J, Jülicher F, Joanny JF (2015) Active gel physics. *Nat Phys* 11:111–117.
29. Storm C, Pastore JJ, MacKintosh FC, Lubensky TC, Janmey PA (2005) Nonlinear elasticity in biological gels. *Nature* 435(7039):191–194.

Supporting Information

Ronceray et al. 10.1073/pnas.1514208113

Methods

Network Energy Minimization. Using the network model described in the main text, we investigate the response to localized active forces of the form $-\mathbf{F}_i \cdot \mathbf{R}_i$, where $\mathbf{R}_i$ is the position of vertex i of the network, as illustrated in Fig. S1. Summing the associated elastic energy with all fiber stretching and bending contributions, our total Hamiltonian reads

$$\mathcal{H} = -\sum_{\text{forces } i} \mathbf{F}_i \cdot \mathbf{R}_i + \sum_{\text{segments } (i,j)} \mu \frac{(\ell_{ij}-1)^2}{2} + \sum_{\text{hinges } (i,j,k)} 2\sin^2\frac{\theta_{ijk}}{2}, \quad \text{[S1]}$$

where ℓ_{ij} is the length of the segment (i,j) linking vertices i and j, θ_{ijk} is the angle formed between two consecutive segments (i,j) and (j,k), and $\mathbf{R}_i$ is the position of vertex i at which the force $\mathbf{F}_i$ is applied. We consider only the athermal equilibrium response of the system, which is obtained by minimizing the total Hamiltonian of the system, using conjugate gradient methods.

Active Stress Measurements. The contractility of our active networks is quantified by the value of its macroscopic active stress. To quantify this stress, we use a framework previously developed by us and suited for the analysis of random discrete networks with next-nearest neighbor interactions (2). This framework includes different prescriptions for systems with fixed and periodic boundary conditions.

For fixed boundary conditions, we compute the system's active stress tensor $\sigma^{\mu\nu}$ from the forces exerted by the network on its boundaries,

$$\sigma^{\mu\nu} = -\frac{1}{V}\sum_{\substack{\text{boundary}\\ \text{sites } i}} f_i^\mu r_i^\nu, \quad \text{[S2]}$$

where the sum runs over the network's boundary sites with positions $\mathbf{r}_i$, $\mathbf{f}_i$ is the force exerted by the network on the boundary at site i, and V is the volume of the system. Note that $\sum f_i^\mu r_i^\nu$ is in fact the force dipole tensor associated with these boundary forces. In the large length-scale limit our active stress tensor $\sigma^{\mu\nu}$ is exactly identical to the active stress tensor appearing in hydrodynamic active gel theories (28).

For periodic boundary conditions (used in Fig. 4 of the main text), we use the so-called mean-stress theorem

$$\sigma^{\mu\nu} = \frac{\Sigma^{\mu\nu}}{V} - \frac{D^{\mu\nu}_{\text{loc}}}{V}, \quad \text{[S3]}$$

where $D^{\mu\nu}_{\text{loc}} = \sum_i F_i^\mu R_i^\nu$ is the force dipole tensor associated with the active forces and $\Sigma^{\mu\nu} = \sum_{i,j} \sigma^{\mu\nu}_{(i,j)}$ is total stress inside the system, given as a function as the discrete stress $\sigma^{\mu\nu}_{(i,j)}$ associated with bond (i,j) (2). Numerical computations of the active stress from Eq. **S3** are straightforward, as both $D^{\mu\nu}_{\text{loc}}$ and $\Sigma^{\mu\nu}$ are readily accessible local quantities.

Measurements of the Rope-Like Region Radius. Our definition of the radius R^* of the rope-like region surrounding an isolated active unit relies on the identification of the crossover of the radial stress $\sigma_{rr}(r)$ between rope-like and linear stress propagation (Eqs. **5** and **6** of the main text). We measure $\sigma_{rr}(r)$ by performing a virtual "cut" of the system in a circular (or spherical in three dimensions) shell and averaging the radial components of the stress (including the bending tension) of all fibers that cross this shell. To this end, we use the discrete stress definition introduced in ref. 2.

The identification of the crossover length is complicated by the fact that the linear regime is not a pure scaling regime. Indeed, it is affected by the boundary conditions of the system. For an isotropic elastic continuum with spherical symmetry, the generic solution to the linear elastic equations for the radial displacement $u_r(r)$ is

$$u_r(r) = Ar^{-(d-1)} + Br, \quad \text{[S4]}$$

where d is the space dimension, and the constants A and B are set by the boundary conditions. The radial stress thus reads

$$\sigma_{rr} = -2d\mu A r^{-d} + 2\mu\frac{1+\nu}{1-(d-1)\nu}B, \quad \text{[S5]}$$

where μ is the shear modulus and ν is the Poisson ratio of the material. In the case of an infinite system, $B=0$ and the linear regime is a pure scaling regime $\sigma_{rr} \propto r^{-d}$. However, in a finite system, any choice of boundary conditions will lead to a finite value for B, thus perturbing the scaling regime and complicating the estimation of R^* [raw value of $\sigma_{rr}(r)$ in Fig. S2].

In the case of fixed boundary conditions, as in Fig. 3 of the main text, we have $B = -A/R^d$, where R is the radius of the system. In addition, the Poisson ratio of elastic fiber networks is easily measured, and we numerically find that it is independent of the precise geometry and connectivity of the network: In $d=2$, $\nu = 3/5$ and in $d=3$, $\nu = 5/13$ (note that these values do not correspond to actual experimental Poisson ratios, but only to idealized fiber networks, and are exact for regular networks). We can thus extrapolate the infinite-system value of the radial stress by subtracting the part due to the fixed boundaries. To avoid issues associated with bonds that intersect the system's boundary, we measure the radial stress at a radius R_1 slightly smaller than R and compute the corrected "infinite system" stress as a function of our finite-size "raw" measurement, using the formula

$$\sigma_{rr}^{(\text{infinite system})}(r) = \sigma_{rr}^{(\text{raw})}(r) - \frac{R_1^d}{R_1^d + gR^d}\,\sigma_{rr}^{(\text{raw})}(R_1), \quad \text{[S6]}$$

where $g = d - d^2\nu/(1+\nu)$. Interestingly, in both $d=2$ and $d=3$ we find $g = 1/2$. The corrected stress exhibits a clear scaling regime in the far field, as demonstrated in Fig. S2, which can then be used to clearly define the rope-like radius R^*.

Experimental Data. As shown in Table 1 of the main text, our predictions on stress amplification are quantitatively supported by a range of experiments in $d=2$ and $d=3$ in reconstituted cytoskeletal as well as extracellular networks. Here we detail the estimates leading to the figures shown in the main text.

Our first example ("system I" in the main text) illustrates the linear regime (Fig. 4 *B* and *G* of the main text) in 3D actomyosin. In ref. 14, a cross-linked actin network with mesh size $\xi = 200$ nm is populated by myosin thick filaments of size $R_0 = 1$ μm, each comprising $\simeq 300$ myosin heads. Each head actively exerts a $f = 4$ pN force 2% of the time (26). Of these 300 heads, half pull in each direction. Furthermore, we use the simplifying assumption that the myosin thick filament is uniformly decorated

with motor heads, and thus the average span of the force dipole is $R_0/2$. This results in a local force dipole $\mathcal{D}_{\rm loc} = -150 \times R_0/2 \times f \times 2\%$ and each thick filament as a whole exerts a typical force $F = \mathcal{D}_{\rm loc}/R_0 \simeq 6$ pN on the network. Actin filaments have a persistence length $\ell_p \simeq 10$ μm, implying a buckling force $F_b \approx \pi^2 k_B T \ell_p/\xi^2 = 10$ pN for a single network bond. As a result, the active unit force is too small to induce filament buckling, and we thus expect linear force transmission in this experiment. Hence $\sigma_{\rm th} = -\rho \mathcal{D}_{\rm loc} = \rho F R_0 \simeq 12$ Pa, where we used $\rho = 2$ μm^{-3}. This number is in very good agreement with the estimation $\sigma_{\rm exp} \simeq 14$ Pa of the macroscopic stress in ref. 14.

Our second example ("system II" in the main text) illustrates force-controlled amplification in 2D actomyosin networks (Fig. 4 *C* and *G* of the main text). Ref. 17 reports active stresses generated by a membrane-supported two-dimensional actomyosin sheet competing with the tension of a bare lipid membrane. This reveals that the active stresses generated by thick filaments ($F \simeq 6$ pN as above) in a 2D actin network ($\xi = R_0 = 1$ μm) covering a giant unilamellar vesicle of radius $r \simeq 10$ μm are of the same order as the tension of the membrane, $\sigma_{\rm exp} \approx \sigma_{\rm membrane} \approx 10^{-6} - 10^{-4}$ N·m^{-1} [the vesicles are electroformed and contain a mixture of egg-phosphatidylcholine (EPC) and biotin-PEG lipids]. The range of tensions given here shows typical values for such vesicles as no direct tension measurements are available in these experiments. The experiments involve an average of three myosin thick filaments per vesicle, implying $\rho = 3/(4\pi r^2) \simeq 2 \times 10^{-3}$ μm^{-2}. Computing the buckling force as $F_b \approx \pi^2 k_B T \ell_p/\xi^2 = 0.4$ pN and assuming a stretching-dominated network, we predict a buckling radius $R^* = R_0 F/F_b = 15$ μm that is both larger than the mesh size and smaller than the intermotor spacing $R_{\rm a.u.} = \rho^{-1/2} \simeq 20$ μm, placing this system in the force-controlled amplification regime (Fig. 4 *C* and *G* of the main text). This yields an amplification factor $\sigma_{\rm th}/\sigma_{\rm lin} = R^*/R_0 \simeq 15$ and an overall 2D active stress $\sigma_{\rm th} = \rho F R^* \simeq 2 \times 10^{-7}$ N·m^{-1}.

Our last example ("system III" in the main text) addresses the density-controlled amplification regime (Fig. 4 *D* and *G* of the main text). We consider stress generation in a reconstituted clot composed of a fibrin network rendered contractile by a concentration $\rho = 3 \times 10^8$ cells·mL^{-1} of blood platelets (18). Atomic force microscopy measurements on individual platelets (4) show that each platelet of size $R_0 = 2$ μm exerts a pulling force $F = 15$ nN, thus yielding a force dipole $\mathcal{D}_{\rm loc} = -Fd = -3 \times 10^{-14}$ N·m (4). The linear prediction for the active stress is thus $\sigma_{\rm lin} = -\rho \mathcal{D}_{\rm loc} \approx 9$ Pa. Comparing this to the experimentally measured active contractile stress $\sigma_{\rm exp} = 150$ Pa generated by a blood clot, we thus find a stress amplification factor $\sigma_{\rm exp}/\sigma_{\rm lin} = 17$. As the microstructure of the fibrin network was not investigated in ref. 18, we assume that the network essentially consists of single fibrin filaments or of small-diameter fibrin bundles and thus estimate a persistence length $\ell_p = 0.5$ μm and a mesh size larger than 200 nm ($\xi \geq 200$ nm) (29). To assess the validity of these estimates, we note that they imply a network shear modulus $G' \approx 6 k_B T \ell_p^2/\xi^5 \simeq 20$ Pa (3), consistent with the value $G' = 70$ Pa reported in ref. 18. They moreover imply a rope-like region size $R^* = \xi (F/F_b)^{1/2} \geq 350$ μm (with $F_b \approx \pi^2 k_B T \ell_p/\xi^2$), much larger than the intercell distance $R_{\rm a.u.} = \rho^{-1/3} \simeq 15$ μm. The rope-like regions of neighboring cells thus interpenetrate, implying density-controlled amplification. In this regime, we predict a contractile stress $\sigma_{\rm th} \simeq 70$ Pa and a stress amplification factor $\sigma_{\rm th}/\sigma_{\rm lin} = R_{\rm a.u.}/R_0 \simeq 8$, in order of magnitude agreement with the experimental result. Note that as system III is deep in the density-controlled regime, this prediction is insensitive to our precise estimates of ℓ_p and ξ.

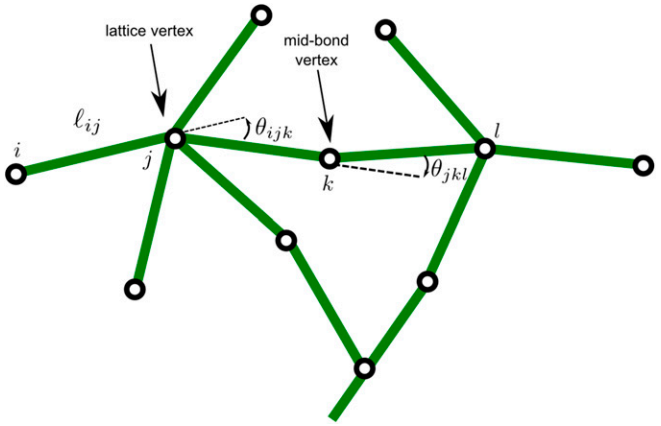

Fig. S1. Schematic representation of the lattice model. The midbond vertices allow buckling of individual bonds.

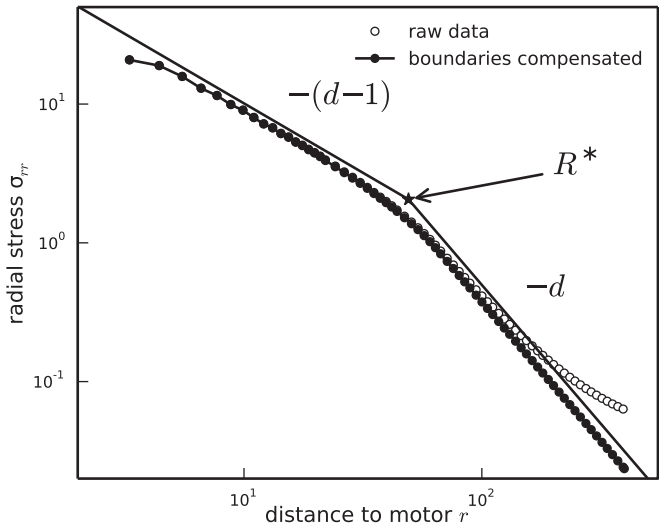

Fig. S2. Compensation of the effect of the fixed boundaries of the system on the spatial distribution of radial stresses.

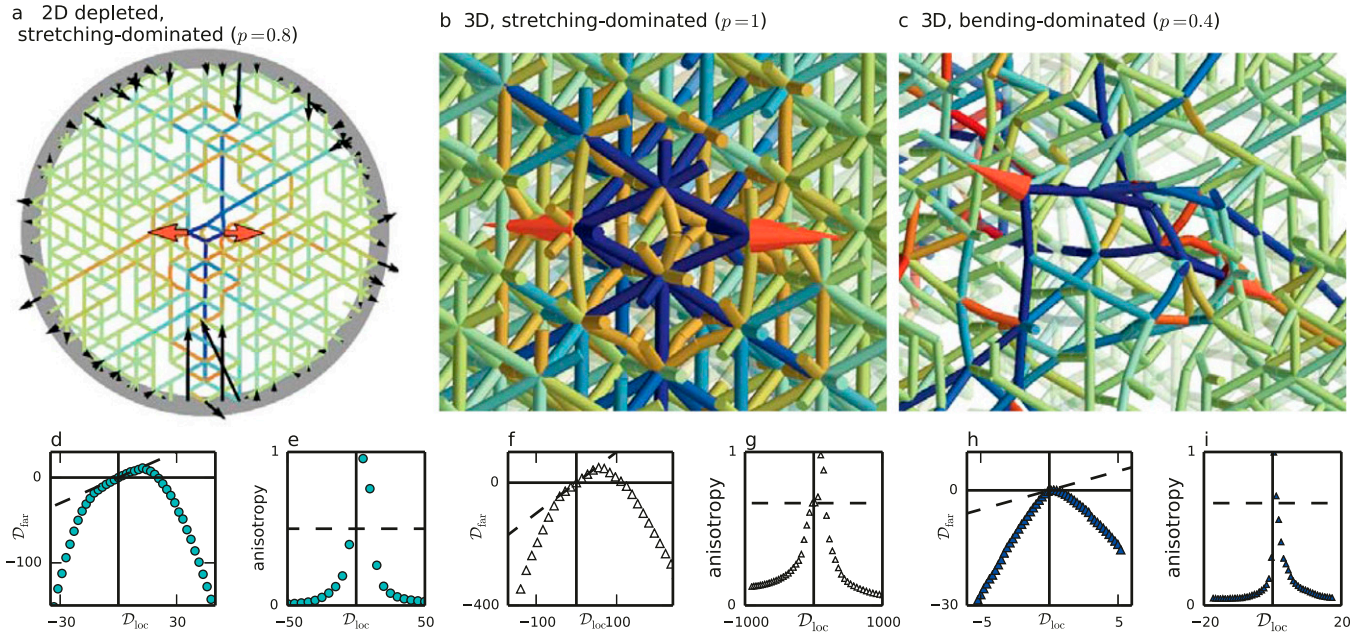

Fig. S3. Rectification, amplification, and isotropization effects are generic features of force transmission in fiber networks. (*A*–*C*) Illustration of the rectification effect in response to an extensile force dipole in various networks. Because compressed segments buckle (red bonds), only tensile stresses (blue bonds) are propagated to the far field. (*D*, *F*, and *H*) The far-field dipole becomes large and contractile for large local force dipoles of either sign. (*E*, *G*, and *I*) The anisotropy of the far-field stress vanishes for large local force dipoles. Note that we apply force dipoles on next-to-nearest neighbors rather than nearest neighbors, such that the two point forces are exerted on distinct fibers. The rationale for this choice is both physical and practical. Physically, cells embedded in extracellular matrix, as well as myosin motors pulling on actin, typically exert forces on different filaments (a myosin thick filament will, for instance, anchor to a pair of actin filaments). Practically, force dipoles applied on nearest-neighbor vertices result in a stress response that is dominated by the very stiff stretching response of the bond joining the two vertices. In such a situation, the response of the system will be dominated by local effects even in the bending-dominated regime, which is both unrealistic and trivial. An alternative option would have been to systematically remove the bond joining the two vertices. However, this biases the network to be locally softer than average, whereas applying the forces on next-to-nearest neighbors does not introduce such a bias.

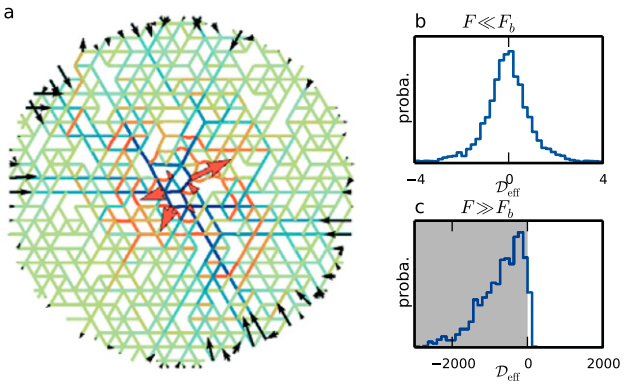

Fig. S4. Rectification of arbitrary local force distributions into far-field contractility. We consider systems where random forces are applied in a small area of seven lattice vertices, with the constraint that the total force and torque vanish. By symmetry, the resulting average local force dipole is equal to zero. (*A*) Typical configuration, showing rectification at large forces. (*B*) The distribution of the effective dipole measured at the boundary in the linear limit ($F \ll F_b$). As expected, the distribution is centered around zero, and the average effective dipole thus vanishes. (*C*) In the large force limit, effective dipoles are overwhelmingly contractile (95% of cases), demonstrating the generality of the rectification effect. Here $p = 0.8$.

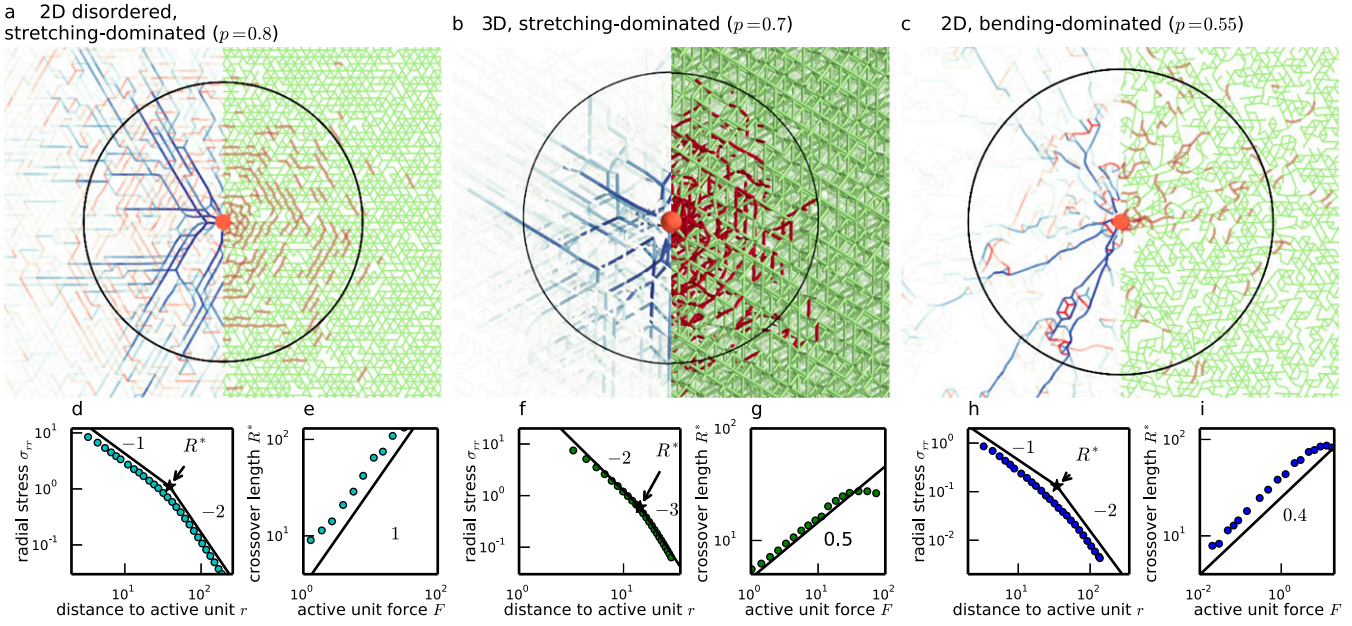

Fig. S5. The force transmission mechanism presented in the main text is insensitive to the specific choice of parameters of the system and in particular to the choice of the depletion parameter *p* characterizing the connectivity of the network. (*A*–*C*) A localized, isotropically pulling active unit (red circle of radius $R_0 = 1.95$) induces stress lines (*A*–*C*, *Left*: blue, tension; red, compression) and buckling (*A*–*C*, *Right*: red, buckling; green, nonbuckled bonds) in the surrounding fiber network. Black circle shows radius *R** of the rope-like region. *B* shows a slice of a 3D system. (*D*, *F*, and *H*) Decay of the average radial stress in the network as a function of the distance to the active unit. (*E*, *G*, and *I*) The exponent α that relates the rope-like radius *R** to the active force *F* depends only on the elasticity regime—stretching or bending dominated—and not on the specific value of *p*. Indeed, $\alpha = 1/(d-1)$ in stretching-dominated networks (*E* and *G*), and the 2D anomalous exponent in bending-dominated networks $\alpha = 0.4$ is reproduced for a lower connectivity than in the main text (*I*). Results were obtained in a circular (spherical) network of radius 200 with fixed boundaries and averaged over 100 samples for disordered networks.

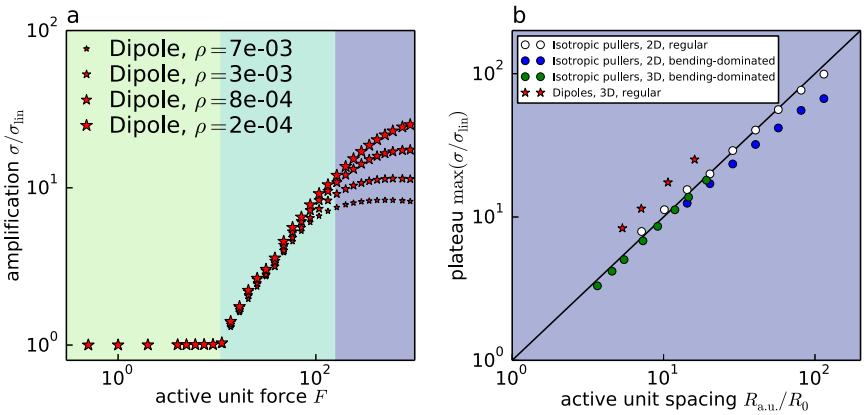

Fig. S6. The stress amplification regimes for a collection of two-point force dipoles of the type used in Fig. 2 of the main text are qualitatively similar to those obtained with isotropically pulling active units (Fig. 4 *A* and *E* of the main text). (*A*) Stress amplification as a function of active force F and active unit density ρ in a regular 3D face-centered cubic network. The three regimes are suggested by the colored background. (*B*) Maximum stress amplification in the large-force regime, as a function of the distance $R_{\mathrm{a.u.}}$ between active units for isotropic pullers (circles) and two-point force dipoles (red stars). Eq. **10** of the main text holds for dipoles as in the analysis of the main text, although here with a prefactor slightly larger than unity.